Theoretical Study of the Electronic States of AlS, AlS^+ and AlS^-

M. Guichemerre and G. Chambaud*

Laboratoire de Chimie Théorique, Université de Marne la Vallée, France

Received: October 18, 1999; In Final Form: December 16, 1999

The spectroscopic constants of the excited doublet and quartet states of AlS have been calculated from potential energy functions obtained by the internally contracted multireference configuration interaction (MRCI) approach. Most of these states have not yet been observed. The shape of the electric dipole and transition moment functions are discussed. The spin−orbit constants and the spin−orbit couplings between different states have been evaluated for those cases in which such couplings are responsible for the perturbations of the spectra. The results are compared with similar data for the isoelectronic AlO. For the low lying electronic states of the AlS cation, the potential energy functions and the spectroscopic constants are reported. The electronic ground state of AlS^- was found to be the only bound state.

I. Introduction

Though aluminum is relatively abundant in outerspace, so far, only two aluminum compounds, AlF and AlCl, have been detected in stellar atmospheres.[1] Model calculations are predicting a similar abundance for metal sulfides such as AlS. The AlS radical or clusters of Al_nS type can be easily obtained from aluminum and sulfur, from Al_2S_3, or from aluminum and traces of sulfur compounds such as CS_2 or OCS under argon atmosphere, and at high temperatures (around 1800 °C). In contrast to numerous theoretical and experimental works for the valence isoelectronic AlO radical (see, for exemple, ref 2), only a few studies were reported for AlS. Except a recent photoelectron spectroscopy study of the AlS^- anion, all experiments were concerned with electronic emission or absorption spectra involving the ground state $X^2\Sigma^+$ of the neutral species.

In 1959, Mc Kinney and Innes[3] detected in the emission spectrum of AlS a band in the region 3700−4800 Å which was attributed to the $A^2\Sigma^+ - X^2\Sigma^+$ transition. Vibrational and rotational constants were determined for both states. This excited state $A^2\Sigma^+$ has also been observed by Maltsev et al.[4]

Kronekvist et al.[5] observed an absorption spectrum in the IR and visible region, which shows evidence of perturbations in the vibrational levels of the $A^2\Sigma^+$ state, but no other transition was detected in this spectral region. The same transition was later studied by Lavendy et al.,[6,7] and they made the assumption that the perturbation stems from the vibrational states of a $^2\Pi$ state lying very close to the ground state with a ω_e close to 500 cm^{-1}. The existence of such a state was confirmed in the photoelectron spectroscopy experiment of Nakajima et al.[8] for AlS^-. This excited $^2\Pi$ state was detected only 0.4 eV above the ground state. In the same experiment, the electron affinity of AlS was determined to be 2.60 eV. The spectroscopic data of the ground state were later improved using high-resolution rotational spectroscopy by Takano et al.[9]

Kronekvist et al.[5] detected in absorption a strongly perturbed $^2\Pi$ excited state in the region 3100−3400 Å and could not decide if this state was regular or inverted. Later, Lavendy detected this excited $B^2\Pi$ state located at about $T_{00} = 30000$ cm^{-1} [10] showing strong perturbations. In the $v = 0$ level, the spin−orbit constant was found to be positive and equal to $A_0 = 117.4$ cm^{-1}.

In the experiments of Maltsev et al.,[4] the excited $C^2\Sigma^+$ state at 35797 cm^{-1} was found to predissociate. The quartet states have neither been studied experimentally nor theoretically. So far, the only theoretical work concerns the ground state of the negative ion and the two low lying doublet states of the neutral by Nakajima et al.[8]

The goal of the present study is to calculate the spectroscopic data of the electronic states of AlS in an energy domain up to 40000 cm^{-1} above the electronic ground state. More than 12 electronic states lie in this region, and most of them correlate with the two lowest dissociation asymptotes. Five low lying electronic states of the cation and the only bound electronic state of the anion AlS^- have also been investigated. Spectroscopic constants, dipole moments, transition dipole functions, and spin−orbit interactions have been calculated. The results are compared with corresponding data of the isoelectronic AlO.

II. Electronic Structure of AlS

The difference in the electronegativities of both atoms (1.61 for Al and 2.58 for S on the Pauling scale) is smaller than in the isoelectronic AlO. However, the ionic character is present in most of the electronic states leading to relatively large dipole moments. For instance, in the electronic ground state of AlS, a dipole moment $\mu_e = 3.63$ D has been calculated. The electronic excitations are often accompanied by strong changes of the ionicity. The proper description of the changes of the ionic character in the electronic states requires very demanding calculations, as in the case of AlO.[2]

Four molecular orbitals (MOs) play an important role in the interpretation of the nature of the electronic states up to 40000 cm^{-1}: (i) the 8σ bonding orbital is a combination of the $3p_\sigma$ orbital of sulfur and of the 3s of aluminum; (ii) the 3π orbital represents mainly the $3p_\pi$ orbital of sulfur; (iii) the nonbonding 9σ orbital is a combination of 3s and $3p_\sigma$ orbitals of aluminum; (iv) the 4π orbital is mainly the $3p_\pi$ orbital of aluminum. The excited states of AlS are essentially described by distributing seven electrons in these four orbitals. The excitation from the valence 7σ orbital leads to electronic states lying higher than 40000 cm^{-1}.

The aim of the present study was to characterize the valence electronic states correlating with the first two dissociation

10.1021/jp993701v CCC: $19.00
Published on Web 02/18/2000

TABLE 1: The Dissociation Asymptotes and the Molecular States of AlS and AlS$^+$

atomic states (Al,S)	energy (eV)[a]	molecular states AlS
$Al(^2P_u) + S(^3P_g)$	0	$^2\Sigma^+$, $^2\Sigma^-$ (2), $^2\Pi$ (2), $^2\Delta$ $^4\Sigma^+$, $^4\Sigma^-$ (2), $^4\Pi$ (2), $^4\Delta$
$Al(^2P_u) + S(^1D_g)$	1.145	$^2\Sigma^+$(2), $^2\Sigma^-$, $^2\Pi$ (3), $^2\Delta$(2), $^2\Phi$
$Al(^2P_u) + S(^1S_g)$	2.75	$^2\Sigma^+$, $^2\Pi$
$Al^+(^1S_g) + S^-(^2P_u)$	3.91	$^2\Sigma^+$, $^2\Pi$
atomic states (Al,S)$^+$	**energy (eV)[a]**	**molecular states AlS$^+$**
$Al^+(^1S_g) + S(^3P_g)$	0	$^3\Sigma^-$, $^3\Pi$
$Al^+(^1S_g) + S(^1D_g)$	1.145	$^1\Delta$, $^1\Pi$, $^1\Sigma^+$

[a] Experimental values.

asymptotes (cf. Table 1). In this table, the energetic position of the first two [$Al^+ + S^-$] asymptotes is also given together with the corresponding molecular states. The attractive electrostatic interaction between both ions brings these two states in the energy region of the first covalent [Al + S] asymptote for an internuclear separation equal or smaller than 7 bohr. As a result, the $A'^2\Pi$ state has almost pure Al^+S^- character in the molecular region. The second $^2\Pi$ state, the $B^2\Pi$ state, lying in the region of the first excited state of Al^+ (configuration 3s3p, at 37392 cm^{-1} above the ground state of Al^+) can be described as a complicated mixture of covalent and excited ionic states. For the $^2\Sigma^+$ symmetry, the situation is more complex; another ionic $^2\Sigma^+$ state with $Al^{2+}S^{2-}$ character can also play a role in the molecular region. Because of the Al^+S^- and $Al^{2+}S^{2-}$ characters of these $^2\Sigma^+$ states, an accurate description requires a balanced multiconfigurational treatment. None of the two lowest $^2\Sigma^+$ states has pure Al^+S^- character or pure $Al^{2+}S^{2-}$ character. At the equilibrium geometry of the $X^2\Sigma^+$ ground state, the $Al^{2+}S^{2-}$ character is dominant, but when the distance increases, its ionicity decreases, simultaneously the ionicity of the $A^2\Sigma^+$ state increases. This has consequences for the variations of the property functions, for instance for the dipole or the transition moments functions (cf. section IV).

III. Computational Details

Calculations were made with the (spdfg) basis set of quintuple-ζ quality (cc-v5z) of Dunning[11] modified by the omission of h functions, corresponding to a total set of 84 contracted Gaussian functions on each atom.

In the CASSCF calculations,[12−14] as for the isoelectronic AlO molecule,[2] we have augmented the valence active space in order to describe accurately all the electronic states of interest as well as their dipole and transition dipole moments. With one additional σ and one additional π molecular orbital, the active space consisted of 11 active molecular orbitals. This space leads to 19234 configurations in $^2\Sigma^+$ symmetry, 19070 in $^2\Pi$ symmetry, and 18856 in $^2\Delta$ symmetry. The MCSCF wave functions for the electronic states were obtained by a state averaged procedure with equal weights for each state.

In the internally contracted multireference configuration interaction (MRCI),[15,16] the reference configurations were selected with a threshold of 0.02 in the configurational expansion of the MCSCF wave function, leading to about 400 configurations as reference wave function for $^2\Sigma$ symmetry, and CI expansions corresponding to almost 3×10^7 uncontracted configurations. In the MRCI calculations, all valence electrons have been correlated. All computations were performed with the MOLPRO code.[17]

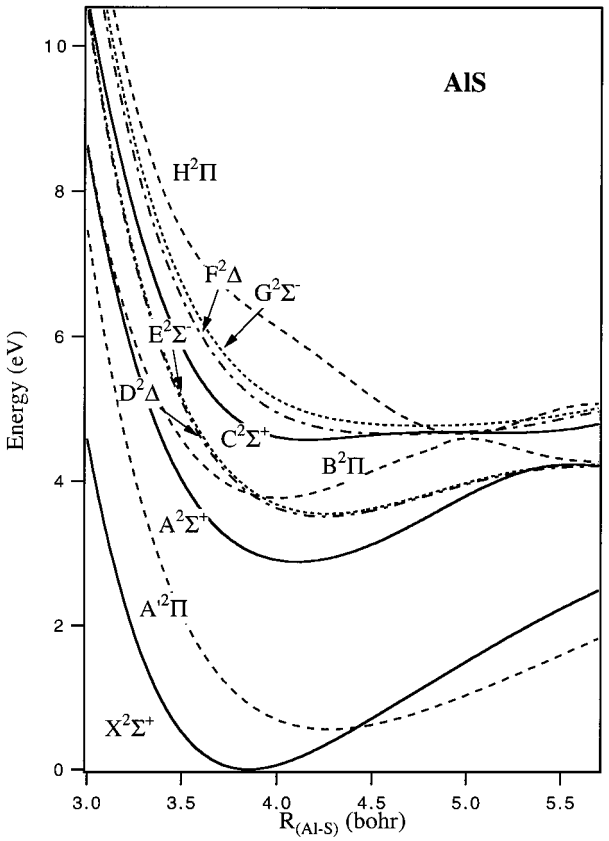

Figure 1. MRCI potential energy functions of the doublet states of AlS.

IV. Discussion of the Results

IV.1. The Doublet States. We have kept the labels of the electronic states as they were previously used, though the alphabetic order does not follow the energetic order, particularly concerned are the $A'^2\Pi$ state[8] and the first set of $^2\Delta$ and $^2\Sigma^-$ states, which are below the observed $B^2\Pi$ and $C^2\Sigma^+$ states.

The potential energy functions obtained by the MRCI approach (averaging 12 electronic states in the MCSCF step) are displayed in Figure 1. The total energy at the equilibrium geometry of the ground state was calculated to be $E_{min} = -639.744788$ au.

The nuclear motion problem has been solved by the Numerov−Cooley method[18] and the calculated spectroscopic constants given in Table 2 are compared with the available experimental or other theoretical values.

For the three lowest electronic states ($X^2\Sigma^+$, $A'^2\Pi$, and $A^2\Sigma^+$), the spectroscopic constants are in good agreement with experiments and previous calculations.[8] The adiabatic excitation energies agree to within ± 0.06 eV with the experiments. The remaining errors are mainly due to the fact that we have averaged a large number of states in the MCSCF step in order to describe highly excited electronic states, and that we have neglected the core-valence electron correlation. The accuracy achieved in these computations for the so far unknown excited states should be similar to that for the states known experimentally.

The variations of the dipole moment of the $X^2\Sigma^+$ and $A^2\Sigma^+$ states with the internuclear separation are shown in Figure 2a. For AlO,[2] it has been found that the dipole moment function of the $X^2\Sigma^+$ state is extremely flat for intermediate distances; the same behavior is found for AlS, but the slope is larger. It is due to the opposite variations of the two terms (the charge q

TABLE 2: Spectroscopic Constants of the Electronic States of AlS, AlS^+, and AlS^-

	states	T_e (cm^{-1})	R_e (Å)	B_e (cm^{-1})	α_e (cm^{-1})	ω_e (cm^{-1})	$\omega_e x_e$ (cm^{-1})	μ_e(debye)	A_{so}(cm^{-1})[g]
AlS	$X^2\Sigma^+$	0	2.04	0.276	0.002	619.74	3.03	3.63	
			2.029[a]	0.2799[a]	0.0018[a]	617.1[a]	3.33[a]		
			2.0315[b]			613.00[b]			
						616.00[c]	3.3[c]		
	$A'^2\Pi$	4372	2.26	0.225	0.002	507.39	3.59	1.07	−307.0
		3200[e]		0.24[d]					
		4839[f]							
	$A^2\Sigma^+$	23152	2.17	0.244	0.001	512.27	1.67	1.23	
		23433[a]	2.164[a]	0.246[a]	0.0012[a]	510.91[a]	1.45[a]		
		23389[e]							
	$a^4\Sigma^+$	23496	2.24	0.230	0.002	440.52	2.90	1.01	
	$b^4\Delta$	25415	2.26	0.226	0.001	426.99	1.25	1.08	
	$c^4\Sigma^-$	26794	2.27	0.223	0.002	436.58	2.83	1.11	
	$D^2\Delta$	28205	2.25	0.228	0.001	480.34	1.22	1.14	168.8
	$E^2\Sigma^-$	28504	2.25	0.228	0.002	458.87	2.69	1.08	
	$B^2\Pi$	30398	2.12	0.256	0.000	571.97	.27	3.14	117.8
		30104[a]							
		29986[a]							
		30001[c]		0.249[c]		559[c]	14[c]		117.4[c]
	$C^2\Sigma^+$	36687	2.21	0.236		465.95		1.15	
		35797	2.19			430			
	$F^2\Delta$	37451	2.46	0.190	0.003	184.94	3.02	−0.36	−301.5
	$G^2\Sigma^-$	38392	2.54	0.178	0.004	184.61	3.77	−0.31	
AlS^+	$^3\Pi$	0[b]	2.17	0.245	0.002	472.83	3.72		
	$^1\Sigma^+$	2019[b]	2.01	0.284	0.002	647.83	3.10		
	$^1\Pi$	2162[b]	2.14	0.252	0.002	541.37	2.63		
	$^3\Sigma^-$	3077[b]	2.91	0.136	0.002	220.47	3.08		
AlS^-	$X^1\Sigma^+$	−19900	2.10	0.263	0.002	513.21	2.90		
		−20969[e]							

[a] Reference 18. [b] Reference 9. [c] Reference 10 ($^2P_{3/2}$ state). [d] Reference 7. [e] Reference 8. [f] Reference 8 (calcd); IE of AlS, 73842 cm^{-1}. [g] Calculated at R_e.

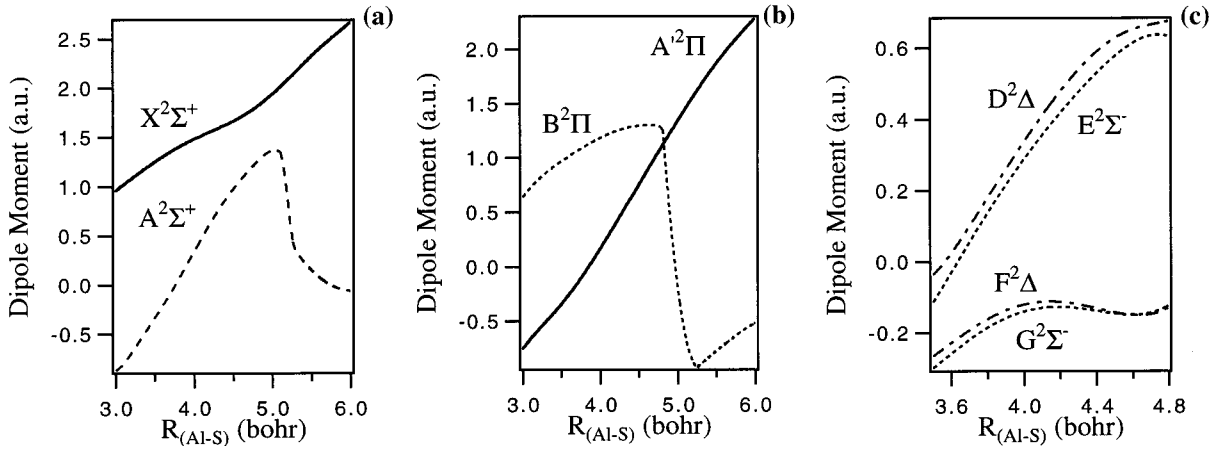

Figure 2. MRCI electric dipole moment functions: (a) of the $X^2\Sigma^+$ and $A^2\Sigma^+$ states of AlS; (b) of the $^2\Pi$ states of AlS; (c) of the $^2\Delta$ states of AlS.

and the distance R) in the dipole moment; the ionic character of the state decreases when the distance increases. As a result, the slope of the dipole function is even smaller than 1. Simultaneously there is a strong increase of the dipole moment of the $A^2\Sigma^+$ state, for the same range of distances, related to the admixture of the $Al^{2+}S^{2-}$ form, yielding a slope of the dipole function larger than 2. The dominant configurations describing both states are $8\sigma^2 3\pi^4 9\sigma^1$ ($Al^{2+}S^{2-}$) and $8\sigma^1 3\pi^4 9\sigma^2$ and $8\sigma^2 3\pi^3 9\sigma^1 4\pi^1$ (Al^+S^-), differing by one electron either in an orbital localized on sulfur (8σ) or in an orbital localized on aluminum (9σ or 4π). Since the orbitals are not completely localized, both states exhibit partial covalent character. The dipole moment of the $A^2\Sigma^+$ state approaches rapidly zero for distances larger than 5.5 bohr, after the avoided crossing with the $C^2\Sigma^+$ state.

The $C^2\Sigma^+$ state forms another avoided crossing with a higher excited state of the same symmetry for R close to 4.3 bohr, leading to a barrier of 0.107 eV relative to the PEF minimum and to strong changes of the dipole moment and of the spin−orbit couplings.

The potential energy curves of the $^2\Pi$ states are given in Figure 1. For the $A'^2\Pi$ state, the main configuration is $8\sigma^2 3\pi^3 9\sigma^2$, corresponding to the ionic Al^+S^- form. The dipole functions of the $^2\Pi$ states (Figure 2b) show a strong change due to an avoided crossing between the $B^2\Pi$ state and the next $^2\Pi$ state for internuclear separations close to 5 bohr. As a result of this avoided crossing, the PEF of the $B^2\Pi$ state possesses a barrier calculated to lie 0.75 eV above its dissociation limit, which is the lowest dissociation asymptote (in contrast to the assumption of Kronekvist et al.[5] that this state dissociates to the second asymptote). The existence of such a barrier explains why excited vibrational levels up to $v = 3$ have been observed[10] even though they are located above the dissociation limit. In the molecular region the $B^2\Pi$ state is strongly multiconfigura-

TABLE 3: MRCI Electronic Transition Moments (in au)

R (bohr)	3.85[a]	4.21[b]
$X^2\Sigma^+-A'^2\Pi$	0.27	0.25
$X^2\Sigma^+-B^2\Pi$	0.50	0.44
$X^2\Sigma^+-A^2\Sigma^+$	0.42	0.32
$X^2\Sigma^+-C^2\Sigma^+$	0.63	0.44
$A'^2\Pi-B^2\Pi$	0.11	0.06
$A'^2\Pi-A^2\Sigma^+$	0.12	0.09
$A'^2\Pi-C^2\Sigma^+$	0.61	0.68
$A'^2\Pi-D^2\Delta$	0.02	0.01
$A'^2\Pi-F^2\Delta$	0.83	0.72
$A'^2\Pi-E^2\Sigma^-$	0.00	0.05
$A'^2\Pi-G^2\Sigma^-$	0.84	0.73

[a] Equilibrium geometry of the $X^2\Sigma^+$ state. [b] Equilibrium geometry of the $A'^2\Pi$ state.

tional with two dominant configurations $8\sigma^2 3\pi^4 4\pi^1$ and $8\sigma^1 9\sigma^1 3\pi^4 4\pi^1$.

In $^2\Delta$ symmetry, we found two low lying states, the $D^2\Delta$ and $F^2\Delta$. There is an avoided crossing between these two states for a distance of 5−6 bohr. The variations of their dipole moments are shown in Figure 2c. The main configuration for both $^2\Delta$ states is $8\sigma^2 3\pi^3 9\sigma^1 4\pi^1$ with three unpaired electrons corresponding to several nonequivalent determinants. Since this configuration differs from that of the $A'^2\Pi$ by one spin−orbital essentially localized at the aluminum atom, the 9σ (mainly $3s,3p_\sigma$) in the $A'^2\Pi$ state and the 4π (mainly $3p_\pi$) in the $^2\Delta$ states, the transition dipole moments between the $A'^2\Pi$ state and these two $^2\Delta$ states should be large. The values of these quantities for two geometries are given in Table 3. The transition dipole moment is large only with the $F^2\Delta$ state and small with the $D^2\Delta$ state, due to different combinations of the nonequivalent determinants describing both Δ states. The same effect was observed in AlO. The MRCI potential of the second $^2\Delta$ state is very flat and the equilibrium distance is large, as for the corresponding state of AlO.

The behavior of the potential functions of the $^2\Sigma^-$ states is very similar to that of the $^2\Delta$ states as shown in Figure 1. The MRCI values of the dipole moments at equilibrium geometry are given in Table 2. As in the case of the $^2\Delta$ states, we found that the transition dipole between the $A'^2\Pi$ state and the $^2\Sigma^-$ states is very small for the first $^2\Sigma^-$ state and rather large for the second one.

The $^2\Phi$ states have been calculated higher than the third $^2\Pi$ state and lying in the Franck−Condon region about 50000 cm^{-1} above the $X^2\Sigma^+$ state.

The variations of some transition dipole functions between the doublet states are shown in Figures 3. The values of the electronic transition moment for all possible transitions, calculated at the equilibrium geometry of the $X^2\Sigma^+$ and $A'^2\Pi$ states are given in Table 3. For the three transitions observed so far, we found that the transition moments have large values.

In Figure 3a one can see that, in the Franck−Condon region, the transition dipole function $R(R)$ for the $A^2\Sigma^+-X^2\Sigma^+$ transition decreases rapidly when the distance increases. Band strengths have been calculated by numerical integration of this electronic transition dipole function between the vibrational states along the internuclear coordinate as

$$S_{v'v''} = |\langle X^2\Sigma^+ \phi_{v''}|R(R)|A^2\Sigma^+ \phi_{v'}\rangle|^2$$

The radiative lifetimes for the first five vibrational levels of the $A^2\Sigma^+$ state have been obtained by inverting the sommation of the Einstein coefficients for spontaneous emission over all the vibrational levels of the $X^2\Sigma^+$ state and the lower vibrational states of the $A^2\Sigma^+$ state, using the same formalism as in ref 19.

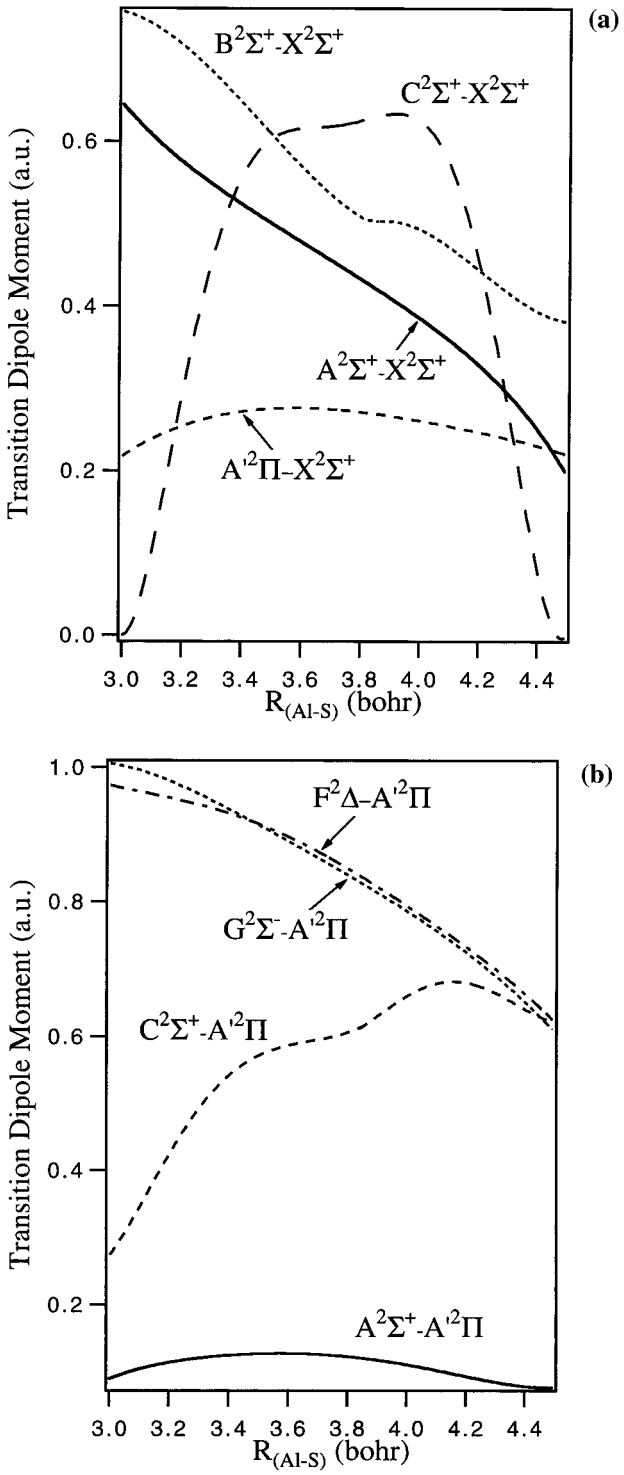

Figure 3. MRCI electronic transition moment functions: (a) between the X state and other doublet states; (b) between the $A'^2\Pi$ state and other doublet states.

We found that the lifetimes are increasing with the vibrational quantum numbers; the calculated values are 720, 749, 778, 808, and 836 ns for the vibrational levels 0−4, respectively. The corresponding lifetimes in AlO are smaller (in the range of 100−130 ns) because the corresponding transition dipole function is larger in AlO than in AlS.

The transition moment function for the $A'^2\Pi-X^2\Sigma^+$ transition exhibits a maximum at about 3.5 bohr but the absolute value is not very large. The transition $C^2\Sigma^+-X^2\Sigma^+$ has a large transition moment in the Franck−Condon region, which rapidly drops in the region of the crossing of the $C^2\Sigma^+$ state with a higher state.

TABLE 4: Spin−Orbit Matrix Elements[a] (in cm^{-1})

	$X^2\Sigma^+$	$A'^2\Pi$	$A^2\Sigma^+$	$B^2\Pi$	$D^2\Delta$	$E^2\Sigma^-$	$C^2\Sigma^+$	$F^2\Delta$	$G^2\Sigma^-$	$^4\Pi$
$X^{2\Sigma+}$ ($r_e = 3.85$)		87.40		66.49		28.95			49.60	39.06
$A'^2\Pi$ ($r_e = 4.21$)		−307.02	97.00	5.88	27.67	26.63	33.42	9.09	0.65	2.92
$A^2\Sigma^+$ ($r_e = 4.10$)				5.01		10.22			49.85	51.72
$B^2\Pi$ ($r_e = 4.01$)				117.8	26.02	27.54	11.85	29.17	30.00	26.95
$D^2\Delta$ ($r_e = 4.23$)					168.78			40.14		34.98
$E^2\Sigma^-$ ($r_e = 4.25$)							13.59			35.73
$C^2\Sigma^+$ ($r_e = 4.18$)									141.18	.87
$F^2\Delta$ ($r_e = 4.65$)								−301.48		41.45
$G^2\Sigma^-$ ($r_e = 4.80$)										43.49
$^4\Pi$ ($r = 4.4$)										40.09

[a] Matrix elements calculated at the geometry (in bohr) given in the first column for each term of the row. $\Delta m_s = 0$ between doublet states, $\Delta m_s = 1$ between doublet and quartet states.

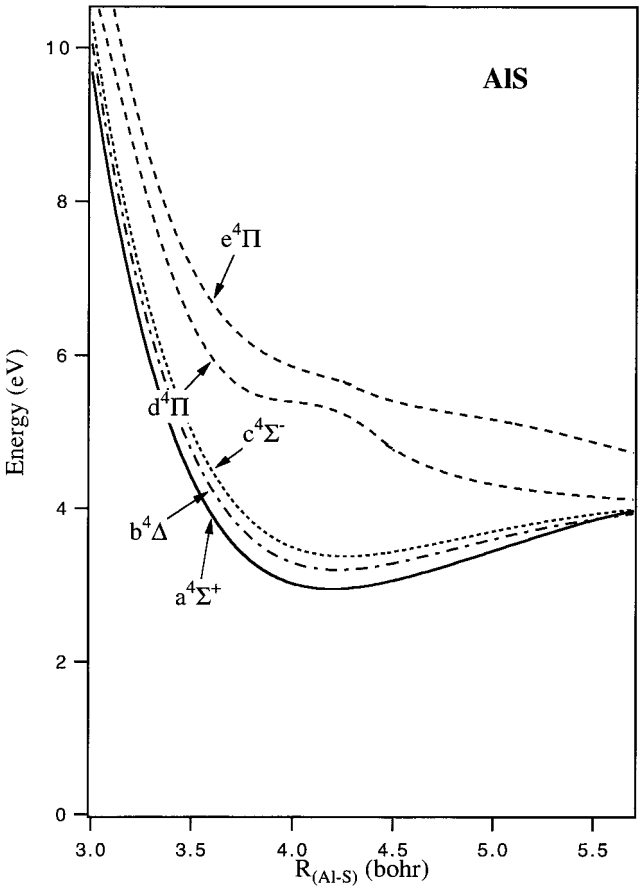

Figure 4. MRCI potential energy functions of the quartet states of AlS.

In Figure 3b, the transition moment functions for the transitions to the $A'^2\Pi$ state are shown. The largest ones are for the two $F^2\Delta-A'^2\Pi$ and $G^2\Sigma^--A'^2\Pi$ transitions. The corresponding $^2\Delta-^2\Pi$ transition has been extensively studied in AlO, but none of these transitions has been observed in AlS. The second intense transition is the $C^2\Sigma^+-A'^2\Pi$ one.

IV.2. The Quartet States. The potential energy functions of the quartet states are shown in Figure 4. The first $^4\Sigma^+$, $^4\Sigma^-$, and $^4\Delta$ states are bound and correspond to the same configuration $8\sigma^2 3\pi^3 9\sigma^1 4\pi^1$ as the $F^2\Delta$ and $G^2\Sigma^-$ states lying in the same energy region. There is only one possible determinant in each quartet symmetry and thus one series of states, contrary to the two series in doublet symmetry ($D^2\Delta$ and $E^2\Sigma^-$ states and $F^2\Delta$ and $G^2\Sigma^-$ states). These bound states are characterized by their spectroscopic constants given in Table 2. The first two $^4\Pi$ states are calculated to be repulsive.

So far, the bound quartet states have not been observed, since the transitions between them are forbidden by symmetry and the transitions to the doublet states are very weak.

IV.3. The Spin−Orbit Couplings. The spin−orbit constants of both atoms have different signs: Al (^{2}P), +74.7 cm^{-1}, and S (^{3}P), − 382 cm^{-1}. Consequently the spin−orbit interactions will be very sensitive to the charge distribution in the radical. All the spin−orbit matrix elements presented here have been calculated from the Cartesian integral of the full Breit−Pauli operator. The wave functions of the three $^2\Sigma^+$ states, the two $^2\Pi$ states, the two $^2\Delta$ states, the two $^2\Sigma^-$ states, and the $^4\Pi$ state have been obtained by state-averaged MCSCF calculations involving all valence electrons in the active space consisting of all the valence orbitals augmented by one orbital in σ and π symmetries.

In Table 4, we give the values of the spin−orbit constants of the electronically degenerate states at equilibrium geometry and the main spin−orbit matrix elements between the electronic states for the equilibrium geometries of one of these states.

The spin−orbit splittings of the $A'^2\Pi$ and $B^2\Pi$ states at equilibrium geometries have been calculated to be −307.0 and +117.8 cm^{-1}, respectively. Our calculated value for the spin−orbit splitting of the $B^2\Pi$ state compares very well with the experimental value of +117.4 cm^{-1}. Previous calculations of Koseki et al.[20] for the $A'^2\Pi$ state give a value of −369 cm^{-1}, which was unfortunately compared with the experimental value for the $B^2\Pi$. Our calculated value for the $A'^2\Pi$ state is certainly more accurate. We can confirm that, as in AlO, the first $^2\Pi$ state is inverted and that the second one is regular. The spin−orbit splitting of the $D^2\Delta$ state has been calculated to be 168.8 cm^{-1} close to its equilibrium geometry and that of the $F^2\Delta$ state to be −301.5 cm^{-1}. As for AlO, the first state is found to be regular and the second one inverted.

In the investigated energy domain, some spin−orbit interactions between doublet states and between doublet and quartet states play a significant role. For instance, in doublet symmetry, the spin−orbit coupling is responsible for the observed perturbations in the $A^2\Sigma^+-X^2\Sigma^+$ spectrum. The couplings of both $^2\Sigma^+$ states with the $A'^2\Pi$ state have been calculated to lie close to 100 cm^{-1}. Their variations with the internuclear distance reflect the changes of the ionicity of the two $^2\Sigma^+$ states (cf. Figure 5a).

The low lying vibrational levels of the $B^2\Pi$ state are perturbed by the close lying $D^2\Delta$ and $E^2\Sigma^-$ states with which the spin−orbit interaction has been calculated to be 27 cm^{-1} in the region of the minimum of the $B^2\Pi$ state. The variations of these couplings with the geometry are presented in Figure 5b. The interaction between the $B^2\Pi$ and the $d^4\Pi$ states has been calculated to be close to 45 cm^{-1} in the region of the crossing of both states. This coupling could also induce perturbations

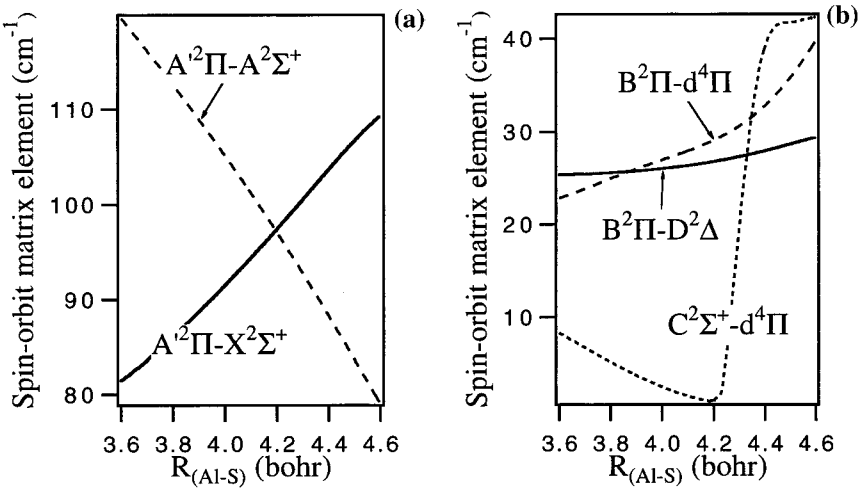

Figure 5. Variations of the spin−orbit interaction: (a) between the A′^{2}Π and the two lowest ^{2}Σ$^+$ states; (b) between the B^{2}Π and the ^{2}Δ state and between the ^{4}Π state and the B^{2}Π and the C^{2}Σ$^+$ state.

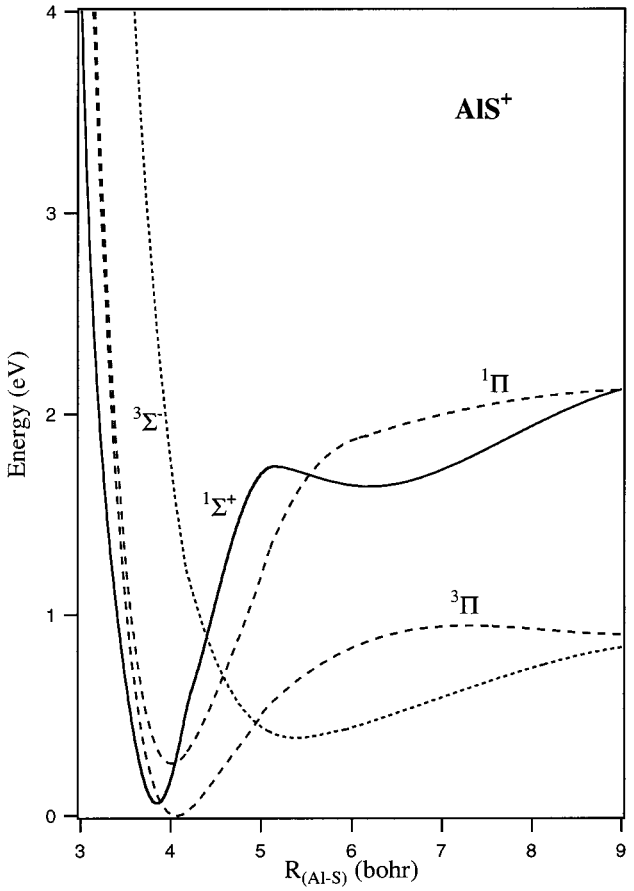

Figure 6. MRCI potential energy functions of the electronic states of AlS$^+$.

and the predissociation of vibrational levels of the B state close to the barrier.

The interaction between the C^{2}Σ$^+$ state and the d^{4}Π state, given in Figure 5b, is small at 4.2 bohr but becomes larger in the region of the crossing of both states explaining the predissociation of the C^{2}Σ$^+$ state.

V. The AlS− Anion

Recently, the photoelectron spectrum of the AlS$^-$ ion has been detected experimentally[8] and the radiation source allowed the observation of the two lowest states (the X^{2}Σ$^+$ and A′^{2}Π states) of AlS. The spectroscopic constants of the electronic X^{1}Σ$^+$ ground state of AlS$^-$ have not yet been reported. Our calculated R_e = 2.10 bohr (cf. Table 2) differs from the equilibrium distances of the X^{2}Σ$^+$ and A′^{2}Π states of AlS, explaining the vibrational progressions observed in the photoelectron spectrum for these states.

The calculated electron affinity of 2.45 eV compares well with the experimental value of 2.60 eV. In a series of additional calculations, we have not found any other bound singlet or triplet state below the detachment threshold.

VI. The AlS$^+$ Cation

We have also studied the five lowest electronic states of the cation correlating adiabatically with its first two dissociation asymptotes. The PEFs of these states are presented in Figure 6, and their spectroscopic constants are given in Table 2.

In contrast to AlO$^+$,[21] the ground state of AlS$^+$ is found to be the ^{3}Π state and not the ^{1}Σ$^+$ state. As shown in Figure 6, the ^{1}Σ$^+$ state exhibits an avoided crossing with another state of the same symmetry for R close to 5 bohr, leading to a second minimum at larger internuclear separation. The ^{3}Σ$^-$ state presents a shallow minimum at large internuclear separation. The ^{1}Δ state is repulsive.

VII. Conclusions

For AlS, AlS$^-$, and AlS$^+$, the PEFs of 17 electronic states were calculated from highly correlated electronic wave functions. The theoretical spectroscopic constants compare very well with those already obtained experimentally for five states. It is expected that the predicted constants for unobserved states will exhibit similar accuracy. The radiative lifetimes of the vibrational levels in the B−X transition have been evaluated from the calculated transition moments. Interpretations of the various perturbations in the electronic spectra are discussed in connection with spin−orbit coupling effects. The results are compared with those of the isoelectronic AlO.

Acknowledgment. The L.C.T. thanks the CEA in Bruyères le Chatel for financial support of this work, and the EEC as part of the TMR network Contract FMRX-CT96088(DG12-BIUO).

References and Notes

(1) Tsuji, T. *Astron. Astrophys.* **1973**, *23*, 411.
(2) Zenouda, C.; Blottiau, P.; Chambaud, G.; Rosmus, P. *J. Mol. Struct. (THEOCHEM)* **1999**, *458*, 61.

(3) MacKinney, C. N.; Innes, K. K. *J. Mol. Spectrosc.* **1959**, *3*, 235.
(4) Maltsev, A. A.; Shevelkov, V. F.; Krupnikov, E. D. *Opt. Spectrosc., Suppl.* **1966**, *2*, 4.
(5) Kronekvist, M.; Lagerqvist, A. *Ark. Fysik* **1968**, *39*, 133.
(6) Lavendy, H.; Mahieu, J.-M.; Bécart, M. *Can. J. Spectrosc.* **1973**, *18*, 13.
(7) Lavendy, H.; Jacquinot, D. *Can. J. Spectrosc*. **1975**, *20*, 141.
(8) Nakajima, A.; Taguwa, T.; Nakao, K.; Hoshino, K.; Iwata, S.; Kaya, K. *J. Chem. Phys.* **1995**, *102*, 660.
(9) Takano, S.; Yamamoto, S.; Saito, S. *J. Chem. Phys.* **1991**, *94*, 3355.
(10) Lavendy, H. *J. Phys. B: Atom. Mol. Phys.* **1980**, *13*, 1151.
(11) Dunning, T. H., Jr. *J. Chem. Phys.* **1989**, *90*, 1007. Wilson, A. K.; van Mourik, T.; Dunning, T. H., Jr. *J. Mol. Struct.* **1996**, *388*, 229.
(12) Roos, B.; Taylor, P.; Siegbahn, P. E. M. *Chem. Phys*. **1980**, *48*, 157.
(13) Werner, H.-J.; Knowles, P. J. *J. Chem. Phys*. **1985**, *82*, 5053.
(14) Knowles, P. J.; Werner, H.-J. *Chem. Phys. Lett*. **1985**, *115*, 259.
(15) Werner, H.-J.; Knowles, P. J. *J. Chem. Phys*. **1988**, *89*, 5803.
(16) Knowles, P. J.; Werner, H.-J. *Chem. Phys. Lett*. **1988**, *145*, 514.
(17) MOLPRO is a package of ab initio programs written by H. J. Werner and P. J. Knowles with contributions of R. D. Amos, A. Berning, D. L. Cooper, M. J. O. Deegan, A. J. Dobbyn, F. Eckert, C. Hampel, T. Leininger, R. Lindh, A. W. Loyd, W. Meyer, M. E. Mura, A. Niclass, P. Palmieri, K. Petersen, R. Pitzer, P. Pulay, G. Rauhut, M. Schuetz, H. Stoll, A. J. Stone, and T. Thorsteinsson. Further details at www.tc.bham.ac.uk/molpro.
(18) Cooley, J. W. *Math. Comput*. **1961**, *15*, 363.
(19) Partridge, H.; Langhoff, S. R.; Lengsfield, III B. H.; Liu, B. *J. Quant. Spectr. Radiat. Transfer* **1983**, *30*, 449.
(20) Koseki, S.; Gordon, M. S.; Schmidt, M. W.; Matsunaga, N. *J. Phys. Chem*. **1995**, *99*, 12764.
(21) Chambaud, G.; Rosmus, P.; Senent, M. L.; Palmieri, P. *Mol. Phys*. **1997**, *92*, 399.